Forensic Science International 266 (2016) 178–184

Contents lists available at ScienceDirect

Forensic Science International

journal homepage: www.elsevier.com/locate/forsciint

How important is it to consider target properties and hematocrit in bloodstain pattern analysis?

Sungu Kim, Yuan Ma, Prashant Agrawal, Daniel Attinger *

Department of Mechanical Engineering, Iowa State University, Ames, IA 50011, USA

ARTICLE INFO

Article history:
Received 3 February 2016
Received in revised form 4 May 2016
Accepted 17 May 2016
Available online 24 May 2016

Keywords:
Bloodstain pattern analysis
Drop impact
Trajectories
Hematocrit
Surface roughness
Wettability

ABSTRACT

Trajectory reconstruction from inspection of bloodstain patterns is relevant to crime scene investigation. While the influence of target properties on trajectory reconstruction has been often qualitatively discussed, it has rarely been quantified. Similarly, a few impact studies measure the viscosity of the blood used in impact experiments. In this work, the impact of blood drops is investigated on targets with a range of surface roughness and surface material. The maximum spreading is characterized using a spreading correlation, which relates the ratio of stain diameter to drop diameter with the non-dimensional numbers Reynolds number and Ohnesorge number. The process for obtaining individual spreading correlations for each of the target substrates and for measuring the viscosity of the respective blood samples is described extensively. The error in estimating the drop release height, associated with using an impact correlation unspecific to the target of interest, is estimated analytically and numerically using experimental data. A similar analysis is done when the hematocrit of the blood is assumed rather than measured. Both assumptions lead to significant errors in estimating the release height of a blood droplet.

1. Introduction

Bloodstain pattern analysis has several applications in crime scene reconstruction, informing on the sequence and timing of the events, their mode of operation, and the location of blood sources. The latter application is known as the determination of the region of origin and involves the inspection of bloodstains and the backward reconstruction of trajectories. Current methodologies for predicting the origin of a bloodletting event rely on assuming that blood drops travel in straight lines [1]. While simple, the technique involves intrinsic inaccuracies since the effect of drag and gravity on drop flight are unaccounted. These inaccuracies become significant as the distance between the origin of the event and the spatter increases, or in specific cases of downward projecting drops [2]. Several extensive studies have also explored the uncertainty associated with an arbitrary selection of stains or the values of impact angles [3–5].

To reconstruct the trajectories backward and account for drag and gravity, knowledge of droplet size and impact velocity is required [6]. These can be estimated from the morphology of the bloodstains, by e.g. analyzing their size, volume and number of spines [7–9]. In this regard, there is significant literature proposing correlations between stain diameters, droplet sizes, and impact velocities [7,10,11]. A few studies have also demonstrated backward reconstruction of trajectories [7,11], albeit without quantifying the influence of specific target properties and blood hematocrit. Blood is indeed a highly complex, shear-thinning, non-Newtonian fluid, whose flow behavior depends on several factors such as: shear rate (or the impact velocity), temperature, hematocrit and humidity [12–14]. Hematocrit values in human blood of healthy individuals vary between values of about 40 to 45% [1,15,16].

This manuscript highlights the effect of varying target conditions in predicting the trajectories of blood drops. The experimental analysis presented here considers dripping drops impacting vertically on glass, cardboard, polycarbonate and aluminum targets. The influence of target wettability and roughness is documented, together with the influence of humidity, room temperature, blood temperature and hematocrit. The study also describes a process to measure the viscosity of blood and to estimate its variation with hematocrit and temperature. The spreading characteristics of the drop, in regards to surface wettability and roughness, are discussed by generating individual correlations for each of the targets. Based on the differences between correlations, the study quantifies the inaccuracies in the simple trajectory reconstruction task of identifying the drop release height when target-independent correlations or population-average hematocrit levels are used instead of values specific to the case at hand.

* Corresponding author at: 2036 Black Engineering, Ames, IA 50011.
Tel.: +1 515 294 1692.
E-mail address: attinger@iastate.edu (D. Attinger).

http://dx.doi.org/10.1016/j.forsciint.2016.05.015
0379-0738/

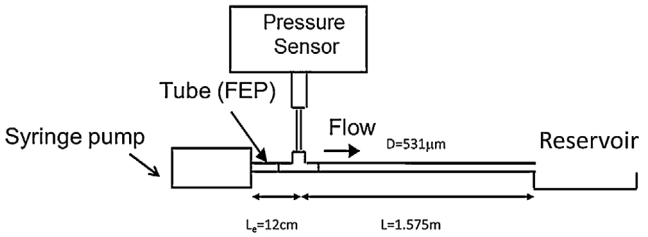

Fig. 1. Before each measurement, the non-Newtonian, shear-thinning viscosity of the blood is measured with a capillary viscometer built according to this schematic.

2. Experimental setup

2.1. Blood handling

For the blood droplet impact studies on solid surfaces, blood from healthy swine is utilized, which is comparable to human blood by its ability to assemble in rouleaux at low shear rates [17,18]. The blood used in this study is purchased from the National Animal Disease Center, in Ames, IA. The anticoagulant used is 1% heparin. Before use, the blood is placed on a rocker (Labquake, Thermo Scientific) until it reaches room temperature. The hematocrit of the blood is measured through centrifugation (STI, HemataStat-II) at 1548–2312 g for 60 ± 3 s, as per the manufacturer's instructions. The temperature of blood, room temperature and relative humidity are also documented prior to experimentation. No blood samples older than three days were used in the experiments.

2.2. Blood rheometry

Before each blood droplet impact experiment, blood viscosity is measured at the documented temperature and at different shear rates (seven measurements are taken with shear rates ranging from 10 to 2500 s^{-1}), using the capillary viscometer setup shown in Fig. 1. The setup comprises a syringe pump (KD Scientific, 780230) which pumps blood into a hard polycarbonate capillary tube (FEP, ID 0.521 mm, length 1.575 m), with a controlled flow rate between 0.01 and 2 mL/min. These values of flow rates correspond to a Reynolds number $Re < 600$, thereby assuring a laminar flow. A differential pressure sensor (Omega DPG 110, with a range of 1 to 7 bar and accuracy < 0.5%) is employed to measure the pressure drop ΔP along the tube at different flow rates Q. The entry length (L_e) for Newtonian flows is theoretically calculated as $L_e/D = 0.06Re$, where D is the internal diameter of the tubing [19]. For $Re = 600$, the entry length for a Newtonian flow comes out to be 18 mm, and that for a shear-thinning fluid is of comparable length [20]. In the experimental setup, an entry length of 12 cm is provided to ensure that the velocity profile is fully developed before reaching the pressure sensor.

The Ostwald-de Waele power-law equation is used to describe the shear-thinning behavior

$$\tau = K\dot{\gamma}^n, \tag{1}$$

with $\dot{\gamma}$ is the shear rate, τ, the shear stress, and K and n the respective flow consistency and non-Newtonian power-law exponent. Then, the Rabinowitsch–Mooney (RM) equation is employed to determine the non-Newtonian shear rate [21,22]:

$$\dot{\gamma} = -\frac{Q}{\pi R^3}\left(3 + \frac{d\log Q}{d\log \Delta P}\right) \tag{2}$$

Above, R is the hydraulic radius of the tubing and d represents the derivative. The non-Newtonian power law exponent (n) is expressed as

$$n = \frac{d\log \Delta P}{d\log Q} \tag{3}$$

Equation (1) is coupled with the wall shear stress (τ_w) given by:

$$\tau_w = \frac{D\Delta P}{4L} = K\dot{\gamma}^n, \tag{4}$$

to calculate the coefficient K. The relative uncertainty (SD = 4%) on the viscosity measurements with the capillary viscometer is mostly due to the uncertainty on the temperature and on the pressure measurement.

The viscosity measurement reaches a plateau (4.1 ± 0.05 mPa·s) above a shear rate of approximately 580 s^{-1}. While the chosen mathematical correlation matches well with the data points in general, there is a slight mismatch where the measured viscosity reaches a plateau due to the inherent mathematical shape of the curve fit. Expressions for the viscosity accounting for the dependency on shear rate, temperature (T) [6] and hematocrit (H) can be obtained as follows. First, the power law curves, equation (5), of six blood samples (labeled A to F), measured at different temperature and hematocrit levels, are tabulated in Table 1.

Then, the viscosity at a given shear rate is expressed as a linear function of T and H, as in

$$\mu(\dot{\gamma}) = a_0 + a_1 T + a_2 H, \tag{5}$$

where, a_0, a_1 and a_2 are coefficients calculated using the method of least squares[23]:

$$\begin{bmatrix} N & \sum_{i=1}^{N} T_i & \sum_{i=1}^{N} H_i \\ \sum_{i=1}^{N} T_i & \sum_{i=1}^{N} T_i^2 & \sum_{i=1}^{N} T_i H_i \\ \sum_{i=1}^{N} H_i & \sum_{i=1}^{N} T_i H_i & \sum_{i=1}^{N} H_i^2 \end{bmatrix} \begin{bmatrix} a_0 \\ a_1 \\ a_2 \end{bmatrix} = \begin{bmatrix} \sum_{i=1}^{N} \mu_i \\ \sum_{i=1}^{N} T_i \mu_i \\ \sum_{i=1}^{N} H_i \mu_i \end{bmatrix} \tag{6}$$

Although the viscosity typically varies exponentially with temperature [19], the small temperature range (15–30 °C) in the present experiments allows a linear assumption between the viscosity and temperature[13].

A question arises as to which shear rate to use for evaluating the viscosity. In drop impacts with relevance to bloodstain pattern analysis, the shear rate is on the order of the impact velocity divided by the drop diameter [7]. Taking a typical case of a 1 mm droplet travelling at 2 m/s or faster, this corresponds to a shear rate of 2000 s^{-1} or larger. Also, as observed in Fig. 2, the viscosity attains a plateau above a shear rate of approximately 580 s^{-1}. This plateau, physically corresponds to the situation where shear is so high that

Table 1
Capillary viscosity measurement at different temperatures and values of hematocrit.

Blood sample No.	Temperature [°C]	H[%]	Viscosity[cP]: measured @ shear rate	Power law fit curve	R^2
A	23.5	42 ± 1	4.29 @1870 s^{-1}	$\mu = 53.485(\dot{\gamma})^{-0.344}$	0.994
B	27	34 ± 1	3.32 @2381 s^{-1}	$\mu = 11.099(\dot{\gamma})^{-0.172}$	0.861
C	27.1	37.5 ± 1	3.57 @2352 s^{-1}	$\mu = 9.193(\dot{\gamma})^{-0.13}$	0.9672
D	26	44 ± 1	4.12 @2472 s^{-1}	$\mu = 8.783(\dot{\gamma})^{-0.106}$	0.9442
E	26	44 ± 1	3.91 @2536 s^{-1}	$\mu = 15.107(\dot{\gamma})^{-0.185}$	0.9713
F	25.6	44 ± 1	4.08 @2479 s^{-1}	$\mu = 9.462(\dot{\gamma})^{-0.116}$	0.9476

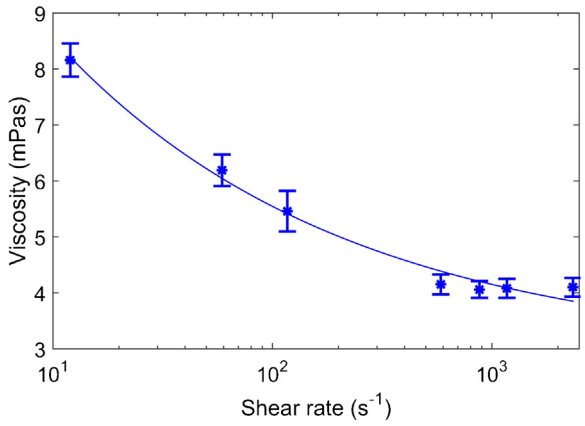

Fig. 2. The viscosity of swine blood as a function of shear rate. The plotted data was obtained at a room temperature of $T = 27.1\,^{\circ}C$, and hematocrit $H = 37.5\%$, corresponding to measurement C in Table 1.

blood cells no longer interact so that the blood assumes Newtonian behavior. Consequently, the blood viscosity value used here is at a shear rate of $2000\,s^{-1}$. As a function of T (in °C) and H (in %), it corresponds to the following correlation

$$\mu(2000) = 2.9155 - 0.0796T + 0.068H. \quad (7)$$

2.3. Drop impacts experiments

As described in Table 2, the drop impact experiments are conducted on glass, cardstock (Colorbok, textured white cardstock), polycarbonate and aluminum surfaces, which represent a range of non-absorbing surfaces. Several values of surface roughness for polycarbonate and aluminum surfaces are obtained after grinding with sand paper and subsequent rinsing with isopropanol and deionized water. Then, to dry the targets, the aluminum surfaces are wiped with clean tissue, while only compressed air is used for polycarbonate to prevent the formation of static charge on the surface.

Surface roughness of the targets is measured using a 3D microscope (Hirox, Digital Microscope, KH-8700). The static contact angle of the blood drops, on the targets, is measured using ImageJ software [24]. A syringe pump (KD Scientific, KDS230) is used to create blood droplets, through FEP tubing and a 27 gauge blunt needle (corresponding to an average droplet diameter of 2.47 mm, and a volume of 7.89 μL), as shown in Fig. 3. Within 70% population interval, the uncertainty on the measured droplet diameter is 3.1%, and 6.2% for impact velocity.

Blood is a complex fluid and the following handling precautions have been useful to reduce experimental uncertainties. The blood is continuously pumped (at 0.1 ml/min), without stopping, to prevent its drying at the needle outlet; drying of blood at the needle outlet has been observed to modify drop diameter over time. Correspondingly, a droplet is generated every 5 s. A small

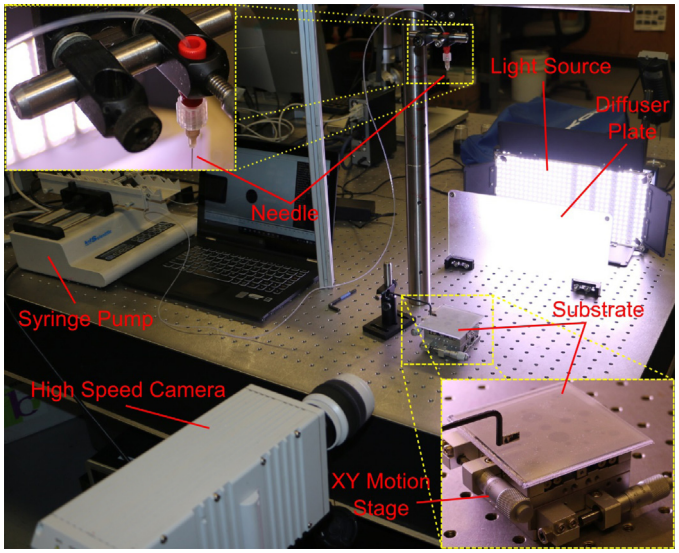

Fig. 3. Experimental setup for conducting blood impact experiments.

container was placed under the needle to collect redundant droplets generated between each trial of experiment. Droplet impact velocity is altered by changing the droplet release height (5, 10, 20, 60 and 150 cm). At each height, the needle is replaced to ensure consistent nozzle condition. The targets are blown with compressed air just before the start of the experiments to remove any residual dust particles. Series of 10 blood stains are created on each surface, at each height, to ensure repeatability of results. A high speed camera (Redlake MotionXtra HG-100 K) is used to record the droplet impact, while the dripping rate is kept constant.

3. Results and discussion

The representative sequence of events during droplet impact and spreading on different targets is shown in Fig. 4. When the droplet impacts normally on the surface, its inertia drives the liquid radially outwards, and this expansion is opposed by viscous dissipation in the blood and by surface tension at the blood–air interface. At t = 2 ms, the droplet stretches the blood into a thin layer called lamella, surrounded by a peripheral thicker ring called the rim. About 3 ms after the impact, as the inertial forces weaken, the droplet reaches a maximum spreading, whereafter capillary and viscous forces dominate. The liquid in the rim is brought back by surface tension toward the vertical axis of symmetry. This recoiling phase occurs for $3\,ms < t < 20\,ms$, and corresponds to the dissipation of the inertial forces by viscous forces. That phase occurs with contact line pinned to the target[7,11,25], except on glass as observed in Fig. 4. After the instance of maximum spreading (image (iv) in Fig. 4), the contact line remains pinned for the aluminium, cardstock and polycarbonate targets, while the contact line on the glass target spreads further: this is attributed to the

Table 2
Blood and target properties used during droplet impact experiment. Viscosity is evaluated considering temperature and hematocrit value. The surface tension and density values are taken and interpolated with respect to temperature from values in [6].

Surface	Polycarbonate bare	Polycarbonate 20 grit	Al mirror	Al 600 grit	Cardstock	Glass slide
Hematocrit (%)	43	43	43	49	49	49
Room temp. (°C)	23.4	23.4	23.1	24.5	24.5	24.5
Blood temp. (°C)	23.5	23.5	23.5	23.2	24.4	24.4
Relative humidity (%)	18.5	18.5	18.5	36.2	56.3	56.3
ρ (kg/m^3)	1060	1060	1060	1060	1060	1060
γ (mN/m)	59	59	59	59	59	59
μ (cP), calibrated	3.97	3.97	3.97	4.41	4.09	4.09

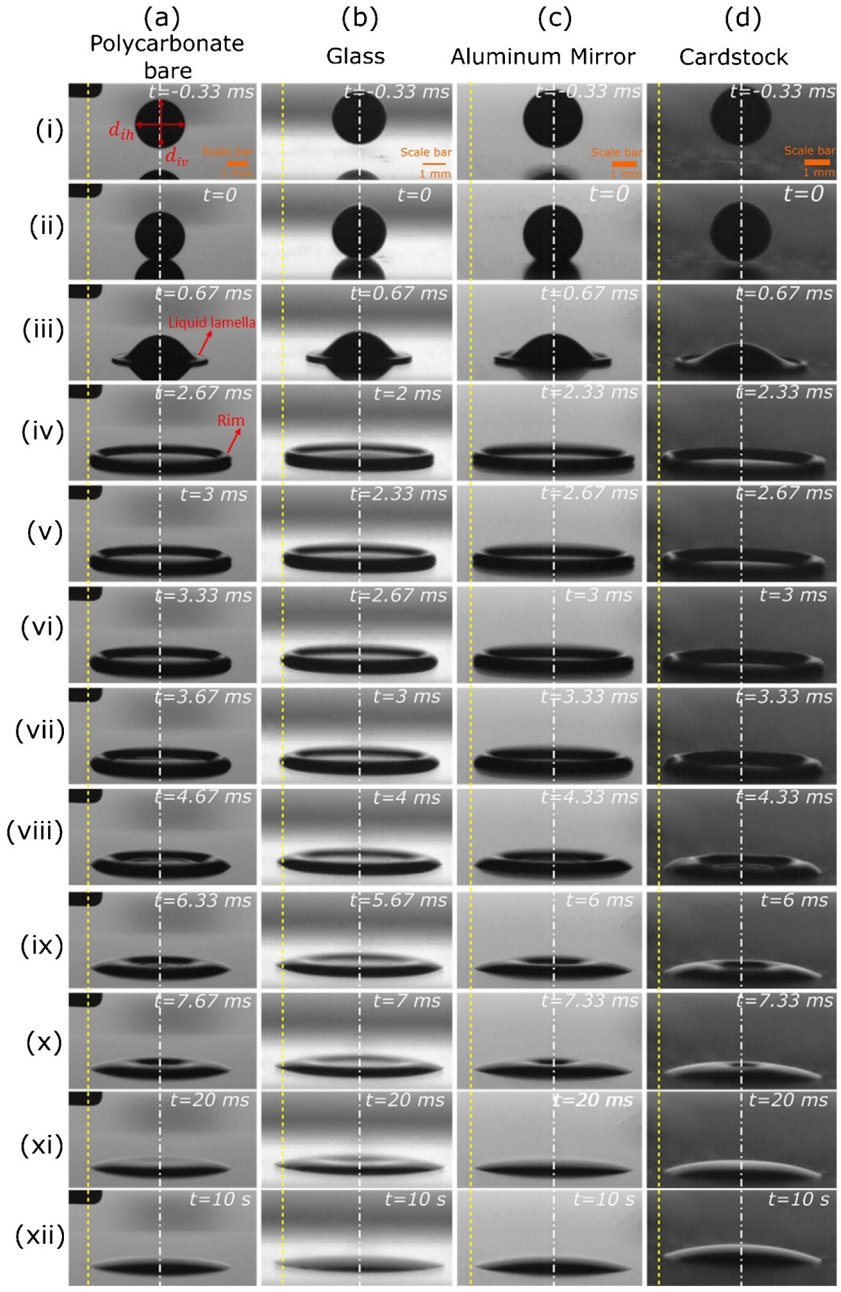

Fig. 4. Evolution of drop spreading on different targets. (a) Polycarbonate bare, (b) Glass, (c) Aluminum, (d) Cardstock. The yellow lines represent the maximum extent of the spreading of the rim. The white lines represent the center of the droplet. The droplet height is 20 cm for all the cases in the figure. Corresponding non-dimensional numbers are: Re = 1200, We = 158 and Oh = 0.010.

significantly higher wettability of the glass target, due to low wetting angle and roughness, compared to the other targets. A glossary for the specific fluid dynamics terms used in this paragraph is available in Tables 2 and 4b of review [6].

To formulate correlations for a specific target, droplet diameter, impact velocity and spreading factor are measured from the sequence of images. Droplet diameter is determined using equation (8), which accounts for drop extensional oscillation following detachment from the needle [26].

$$d_{\mathrm{i}} = \left(d_{\mathrm{ih}}^2 d_{\mathrm{iv}}\right)^{1/3}. \tag{8}$$

Here, d_{ih} and d_{iv} are the horizontal and vertical diameter of the drop in an image. The droplet's impact velocity (V_{i}) is measured by considering the difference in height of the center of the droplets (Δs) between two frames (i and ii in Fig. 4) just before the impact of the drop, and calculated as:

$$V_{\mathrm{i}} = \frac{\Delta s}{\Delta t}, \tag{9}$$

where, Δt is the time difference between the two frames. After the impact, the droplets are left for drying (for about 24 h), and the diameter of the dried stain (D_{S}) is measured to calculate the spreading factor (β).

$$\beta = \frac{D_{\mathrm{S}}}{d_i}. \tag{10}$$

It is noteworthy to mention here that the dried stain diameter is observed to be approximately 2–3% smaller than the blood stain diameter after 20 ms of impact, for all the targets used in the experiments. Having obtained the spreading factor, the impact velocity and diameter, we fit correlations [27] of the

Table 3
Experimental correlations for different targets plotted in Fig.5.

Target	Contact angle (°)	Surface roughness, Ra(mm)	Correlation
Glass	16.1	–	$\beta = 0.8474(Re^2Oh)^{0.1334}$
Aluminum mirror	87.1	0.32	$\beta = 0.4285(Re^2Oh)^{0.1934}$
Aluminum P600 grit	62.2	0.4	$\beta = 0.3914(Re^2Oh)^{0.1965}$
Cardstock	96.8	1.09	$\beta = 0.4019(Re^2Oh)^{0.1921}$
Polycarbonate bare	86.9	0.22	$\beta = 0.3428(Re^2Oh)^{0.2118}$
Polycarbonate P20 grit	98.6	4.5	$\beta = 0.3954(Re^2Oh)^{0.1912}$

Bousfield-Scheller type on each dataset related to an specific target, to characterize the spreading as a function of the impact conditions. This type of correlations are chosen because of their ability to fit a wide range of impact velocities, targets and liquids[27], and for their mathematical simplicity, with

$$\beta = a(Re^2Oh)^b, with\, Re^2OH = \frac{\rho^{1.5} d_i^{1.5} V_i^2}{\mu\sqrt{\sigma}}. \quad (11)$$

Above, a and b are the coefficients of the Bousfield correlation that can be found from curve fitting of the experimental data. Re is the Reynolds number and Oh is the Ohnseorge number given by:

$$Re = \frac{\rho V_i d_i}{\mu} \quad (12)$$

$$Oh = \frac{\sqrt{We}}{Re} \quad (13)$$

Here, We is the Weber number ($We = \rho V_i d_i^2/\gamma$).

The Ohnesorge number can be understood as a comparison between the kinetic energy of impact with the resistant work of the viscous forces and the surface tension. As mentioned previously, as the time scale of the spreading process is extremely small, droplet spreading is associated with high shear rates. Consequently, it is acceptable to employ the viscosity of blood at high shear rates[7]; here, the viscosity value at 2000 s^{-1} is used, as mentioned in Table 3. The corresponding correlations for the different targets are plotted in Fig. 5 and tabulated in Table 3.

Inspection of Fig. 5 reveals first how much larger the spreading is on the glass target. At low impact velocities, the spread factor on glass is on average 25% larger than on the other targets. This might be due to enhanced wetting on the glass, which has a significantly lower contact angle than other targets, as shown in tabulated in Table 3. As the Ohnesorge number increases, i.e. as the ratio of impact energy versus the work of resistance forces increases, the spread factor on the glass target becomes comparable with that on other targets, owing to the decreased influence of wetting forces on spreading[10].

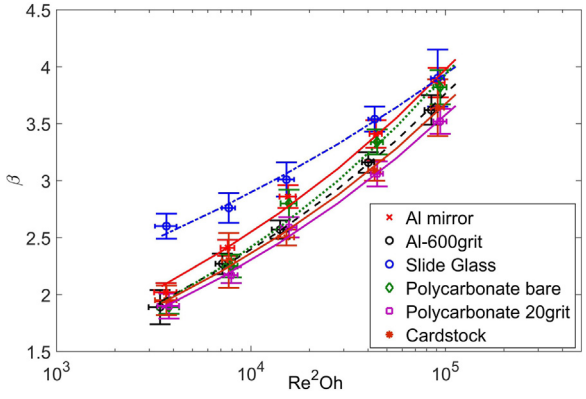

Fig. 5. Experimental correlations between the spreading factor and the non-dimensional number ***Re²Oh***, as a function of the target. The correlations are tabulated in Table 3.

Fig. 5 also demonstrates how spreading is influenced by the roughness, for a given surface. The spreading factor for the roughened aluminum and polycarbonate targets are lower than for their respective unaltered counterparts. These observations are coherent with the observations in Patil et al. [28] and Hulse-Smith et al. [7], where an increase in the surface roughness reduces spreading upon drop impact. The associated formation of spines observed in [7] is attributed to the Rayleigh-Taylor instability, which is encountered when a liquid-air interface is subjected to a sudden acceleration[7,29]. One question that arises is if the spreading factor as calculated by equation (10) remains constant between a few seconds after impact and the hours or days that separate a crime from a thorough bloodstain pattern analysis. Indeed, Brutin et al. [14] recently reported a slow spreading of sessile blood drops on glass due to evaporation, until equilibrium is reached. However, such a spreading is not observed in our experiments of impacting drops. For glass, the dried stain diameter measured 24 h after impact is approximately 2% smaller than the diameter of the blood drop after 20 ms of impact. A similar variation is observed for the other targets, where the dried stain diameter is approximately 2–3% smaller than the blood drop diameter after 20 ms of impact. This difference in spreading behavior, between the observation of Brutin's group, who used sessile drops spreading slowly, and our experiments, can be attributed to the enhanced inertial spreading of the drop on impact in our study, where the inertia of the impacting drops completely overpowers the surface forces and causes the drops to reach a maximum spread within just 20 ms after impact. The spreading induced by evaporative flux observed in [14] is effective on a much larger time scale (in the order of 1 s), hence, its effects are not observed.

Based on the data in Fig. 5, a question of high relevance to forensic arises as follows. *For the purpose of trajectory reconstruction from inspection of stains, can we use a single spreading correlation independently of the target material and conditions?* Let us first quantify the uncertainty on trajectory reconstruction induced by using a one-size fit all correlation, versus correlations specific to a given target. A way to study these effects is by analytical inspection of equation (11). For a given correlation (i.e., known values of a and b) and a known β (from known stain size and drop volume), the height from which the drop is released can be predicted using equation (11). Assuming that drag does not affect the droplet trajectory, the impact velocity of the drop can be given as:

$$V_i = \sqrt{2gh}, \quad (14)$$

where, g is the acceleration due to gravity and h is the predicted drop release height. Using equation (14), equation (11) is transformed into:

$$\beta = a\left(2gh\frac{\rho^2 d_i^2}{\mu^2}Oh\right)^b, \quad (15)$$

from which the drop release height h can be expressed as

$$h = \frac{\mu\sqrt{\sigma}}{2gp^{1.5}d_i^{1.5}}\left(\frac{\beta}{a}\right)^{\frac{1}{b}}. \quad (16)$$

To ascertain the variation in the drop release height prediction originating from variations in a and b, Δh can be written as:

$$\Delta h = \frac{\partial h}{\partial a}\Delta a + \frac{\partial h}{\partial b}\Delta b. \quad (17)$$

The corresponding partial derivatives of equation (16) give:

$$\frac{\Delta h}{h} = -\frac{\Delta a}{ab} + \ln\left(\frac{a}{\beta}\right)\frac{\Delta b}{b^2}. \quad (18)$$

Taking the values for a and b for aluminum mirror as the base, and $\beta = 3$, a 10% change in a (keeping b constant) leads to about a 51% change in h, whilst, a 10% change in b (keeping a constant) leads to about a 43% change in h. Conversely, to ensure that a change in h does not exceed 10% (i.e. $\Delta h/h < 10\%$), the maximum change in a and b should not exceed approximately 2 and 3%, respectively. Relating these observations to the correlations for different targets in Table 3, the variations in a (between 2 and 116%) and b (between 1.5 and 33%) exceed the above calculated values, thereby indicating that a single correlation will significantly impact the prediction of a drop release height.

The effects of this finding can be shown from the current set of experiments, in Fig. 6. Here, we use the measured spread factor β from drop impact experiments on the aluminum mirror target (from all drop release heights), and calculate the drop release height using the spreading correlations of Table 3 specific to each of the targets. For the case with gravity and without drag, equation (16) is used to reconstruct the trajectory. For the case with gravity and drag, the differential equations of motion in [6] are numerically integrated. Hence, the height ratio H_R compares the calculated heights using correlations of the individual targets (x-axis), to the experimental drop release height on the aluminum mirror. It is important to mention here that the data in Fig. 6 corresponds to all the drop release heights used in the experiments (i.e. 5, 10, 20, 60 and 150 cm). Fig. 6 clearly shows a marked difference in height predictions from the respective correlations; the variation in the average height values are tabulated in Table 4. For example, estimating the height of release of stains found on an aluminim mirror target using correlations obtained on glass would underestimate the release height by about 50%, while using correlations for rough polycarbonate would overestimate the height by about 50%.

A related question of interest is the influence of the assumed hematocrit level on the backward reconstruction of trajectories. This corresponds to a crime scene reconstruction where a standard hematocrit level, say 44%, would be used to estimate the height of a released drop, instead of measuring the hematocrit of the individual to whom the blood belongs. For the case where gravity is considered and drag neglected, the resulting uncertainty on the prediction of the release height of a dripping drop can be estimated again by analyzing how equation (16) depends on the hematocrit. First, the viscosity μ of the blood depends on the blood hematocrit, as per equation (5). Second, the drop impact diameter d_i is not known on a crime scene, contrary to the laboratory experiments here where it can be measured from high-speed videos. In a crime scene situation, it has been proposed to estimate d_i by e.g. by measuring the volume V_s of solid material remaining in the stain [6], which is linearly proportional to the drop volume and the hematocrit [9], so that $V_d = \alpha V_s/H$, where α is a proportionality coefficient determined experimentally. For the present experiments, where average drop volume of 7.89 μL and the average value of $H = 44\%$ is known, we have $\alpha V_S = 3.47$ μL. As a result, the estimated impacting drop diameter (d_i), for an unknown value of H can be obtained as:

$$d_i = \left(\frac{6\alpha V_S}{\pi H}\right)^{\frac{1}{3}}. \tag{19}$$

Therefore, using standard values of hematocrit in trajectory reconstruction introduces two systematic errors, one on the blood viscosity and the other on the estimated impact diameter. An example of the systematic error due to the use of standard values of hematocrit for the estimation of the dripping drop release height is shown in Fig. 7 for the situation when a dripping drop impacts an aluminum mirror surface (i.e. $a = 0.4285$ and $b = 0.1934$), with typical spreading $\beta = 3$ and 3.9. The droplet release height was estimated with and without considering the drag force acting on the droplet, as was done for Fig. 6. For a typical hematocrit value of 44%, the estimated droplet release heights are 26.0 cm without drag and 28.1 cm with drag for the spreading factor $\beta = 3$. For the spreading factor $\beta = 3.9$, the estimated droplet release heights are 100.8 cm without drag and 129.8 cm with drag.

The range of height over which the above graph is plotted corresponds to the typical values of hematocrit found in humans. It is seen that within this range, and for this specific trajectory reconstruction task, a difference of 10% between the hematocrit used to develop the correlations, and that relevant to the crime scene (for instance 40% vs. 50%) leads to errors larger than 30% in the

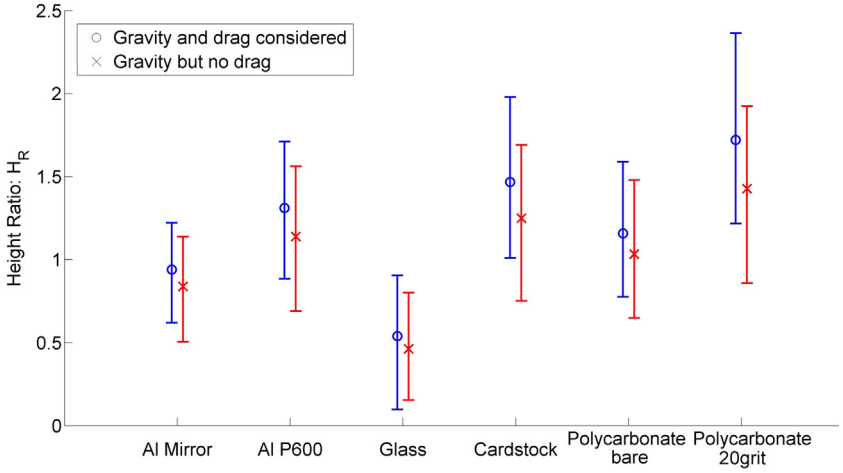

Fig. 6. Comparison of the ratio (H_R) of estimated drop height to the experimental drop height using correlations of different targets for drop impact on aluminum mirror. All the droplet release heights used in the experiment (i.e. 5, 10, 20, 60 and 150 cm) were taken as the reference height to calculate H_R. The drop release heights were calculated with and without considering drag force on the droplet.

Table 4
Comparison of error in average values of H_R from β correlations of different targets.

	Al P600 grit	Glass	Cardstock	Polycarbonate bare	Polycarbonate P20 grit
Drag considered	31.1%	46.9%	46.77%	15.8%	72.1%
Drag not considered	37.7%	71.4%	35.03%	61.8%	44.9%

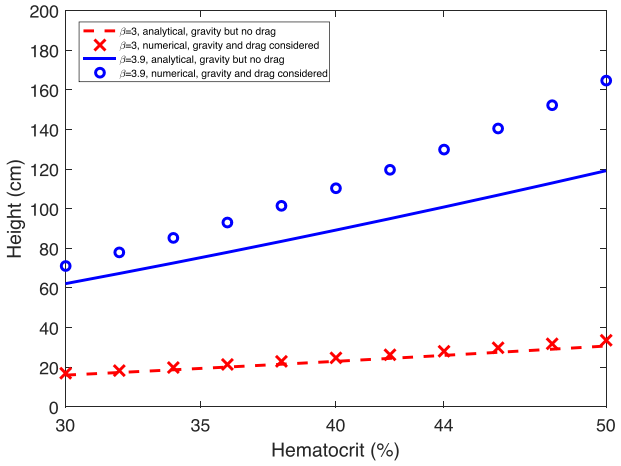

Fig. 7. Variation of the estimated droplet release height for a spreading factor $\beta = 3$ and 3.9, assuming 44% hematocrit, as a function of the actual value of hematocrit. The droplet release height was estimated with and without considering the drag force acting on the droplet.

drop release height calculations (23.0 cm vs. 30.7 cm for $\beta = 3$, 89.2 cm vs. 119.1 cm for $\beta = 3.9$ for calculations without drag). For trajectory reconstructions involving gravity and drag, the error is between 30 and 50% (24.7 cm vs. 33.7 cm for =3; 110.2 cm vs. 164.6 cm for $\beta = 3.9$). Thus, the problem of reconstructing trajectories by inspection of individual drops seems very sensitive to the correct choice of the spreading correlation and to the correct knowledge of the hematocrit.

4. Conclusion

The impact of blood drops on targets with different materials and roughnesses was investigated, detailing a methodology for measuring the viscosity of blood at relevant high shear rates of 2000 s^{-1}. Care was taken to ensure consistent blood flow conditions during experimentation, whilst the blood rheometry procedure allowed the use of appropriate values of blood viscosity for the blood sample used for experimentation, incorporating the effect of temperature and hematocrit. Individual correlations, relating stain size (through spreading factor β) and velocity of impact (through Re^2Oh), were developed for each of the targets, with an aim to minimize the error in calculation of drop release height. Consequently, it was demonstrated, both analytically and numerically, that reconstructing the height of release of an individual drop by stain inspection using correlations obtained with a different target than the target of interest can lead to significant errors, as large as 50% of the drop release height. A similar analysis showed that a difference of 10% between the hematocrit used to develop the correlations, and that relevant to the crime scene (for instance 40% vs. 50%), induced errors between 30 and 50% in the drop release height. The systematic errors induced by misestimating the hematocrit or by using spreading correlations not specific to the target of interest were found larger when drag was included in the calculations, besides gravity. While this level of uncertainty is probably acceptable in most court cases, it is nonetheless important that BPA analysts are aware of the magnitude of the uncertainty. This is especially important in relation with the 2009 study of the US National Academies of Science and Engineering, which mentioned that "the uncertainties associated with bloodstain pattern analysis are enormous" [30]. As a result, we suggest that for an accurate trajectory reconstruction of blood drops, it is advisable to generate correlations individual to the specific surface and blood, if the surface characteristics and hematocrit of the blood specific to the crime scene is available. Employing generalized correlations or average hematocrit levels can lead to significant errors in determining the region of origin of the blood spatter.

Acknowledgments

The authors gratefully acknowledge financial support from the US National Institute of Justice (awards number: 2010-DN-BX-K203, 2014-DN-BX-K036). The authors would also like to thank collaborators Patrick Comiskey and Alexander Yarin for their editorial help, and the latter for also sharing information on blood rheometry, as well as Arpa Ghosh and Basant Sikarwar for contributing to the design of the capillary viscometer.

References

[1] T. Bevel, R.M. Gardner, Bloodstain pattern analysis with an introduction to crime scene reconstruction, CRC Press, Boca Raton, FL, USA, 2008.
[2] K.G. de Bruin, R.D. Stoel, J.C.M. Limborgh, Improving the point of origin determination in bloodstain pattern analysis, J. Forensic Sci. 56 (2011) 1476–1482.
[3] W.F. Rowe, Errors in the determination of the point of origin of bloodstains, Forensic Sci. Int. 161 (Aug 2006) 47–51.
[4] C. Connolly, M. Illes, J. Fraser, Affect of impact angle variations on area of origin determination in bloodstain pattern analysis, Forensic Sci. Int. 223 (2012) 233–240.
[5] M. Illes, M. Boué, Investigation of a model for stain selection in bloodstain pattern analysis, Can. Soc. Forensic Sci. J. 44 (2011) 1–12.
[6] D. Attinger, C. Moore, A. Donaldson, A. Jafari, H.A. Stone, Fluid dynamics topics in bloodstain pattern analysis: comparative review and research opportunities, Forensic Sci. Int. 231 (2013) 375–396.
[7] L. Hulse-Smith, N.Z. Mehdizadeh, S. Chandra, Deducing drop size and impact velocity from circular bloodstains, J. Forensic. Sci. 50 (2005) 54–63.
[8] L. Hulse-Smith, M. Illes, A blind trial evaluation of a crime scene methodology for deducing impact velocity and droplet size from circular bloodstains, J. Forensic. Sci. 52 (Jan 2007) 65–69.
[9] N. Laan, R.H. Bremmer, M.C. Aalders, K.G. de Bruin, Volume determination of fresh and dried bloodstains by means of optical coherence tomography, J. Forensic. Sci. 59 (Jan 2014) 34–41.
[10] C.D. Adam, Fundamental studies of bloodstain formation and characteristics, Forensic Sci. Int. 219 (June 2012) 76–87.
[11] N. Laan, K.G. de Bruin, D. Bartolo, C. Josserand, D. Bonn, Maximum diameter of impacting liquid droplets, Phys. Rev. Appl. 2 (2014).
[12] J. Rosina, E. Kvasnak, D. Suta, H. Kolarova, J. Malek, L. Krajci, Temperature dependence of blood surface tension, Physiol. Res. 56 (2007) S93–S98.
[13] M. Maffesoli, Ritual and daily life as basis of life histories, Cah. Int. Sociol. 69 (1980) 341–349.
[14] W. Bou-Zeid, D. Brutin, Effect of relative humidity on the spreading dynamics of sessile drops of blood, Colloids Surf. A Physicochem. Eng. Asp. 456 (2014) 273–285.
[15] M. Raymond, E. Smith, J. Liesegang, The physical properties of blood–forensic considerations, Sci. Justice 36 (1996) 153–160.
[16] H.L. MacDonell, Bloodstain patterns, 2nd. ed., Laboratory of Forensic Sciences, Corning, NY USA, 2005.
[17] N. Behrooz, L. Hulse-Smith, S. Chandra, An evaluation of the underlying mechanisms of bloodstain pattern analysis error, J. Forensic Sci. 56 (Sep 2011) 1136–1142.
[18] U. Windberger, A. Bartholovitsch, R. Plasenzotti, K.J. Korak, G. Heinze, Whole blood viscosity, plasma viscosity and erythrocyte aggregation in nine mammalian species: reference values and comparison of data, Exp. Physiol. 88 (2003) 431–440.
[19] M.E. Falagas, E.I. Pitsouni, G.A. Malietzis, G. Pappas, Comparison of PubMed, Scopus, Web of Science, and Google Scholar: strengths and weaknesses, FASEB J. 22 (Feb 2008) 338–342.
[20] R.J. Poole, B.S. Ridley, Development-length requirements for fully developed Laminar pipe flow of inelastic non-Newtonian liquids, J. Fluid. Eng.-T. Asme 129 (Oct 2007) 1281–1287.
[21] C. Tropea, A.L. Yarin, J.F. Foss, Springer handbook of experimental fluid mechanics, Springer, Heidelberg, Germany, 2007.
[22] J.F. Steffe, Rheological methods in food process Engineering, Freeman Press, USA, 1996.
[23] S.C. Chapra, R. Canale, Numerical methods for engineers, McGraw-Hill, Inc., 2006.
[24] C.A. Schneider, W.S. Rasband, K.W. Eliceiri, NIH Image to ImageJ: 25 years of image analysis, Nat. Methods 9 (2012) 671–675.
[25] C. Hurth, R. Bhardwaj, C. Frankiewicz, A. Dobos, D. Attinger, F. Zenhausern, Biomolecular interactions control coffee ring effect during droplet drying, Colloids Surf. B Biointerfaces (2014).
[26] A. Rozhkov, B. Prunet-Foch, M. Vignes-Adler, Impact of drops of polymer solutions on small targets, Phys. Fluids 15 (2003) 2006.
[27] B.L. Scheller, D.W. Bousfield, Newtonian drop impact with a solid surface, AIChE J. 41 (1995) 1357–1367.
[28] N.D. Patil, R. Bhardwaj, A. Sharma, Droplet impact dynamics on micropillared hydrophobic surfaces, Exp. Therm. Fluid. Sci. 74 (2016) 195–206.
[29] R.F. Allen, The role of surface tension in splashing, J. Colloid Interface Sci. 51 (1975) 350–351.
[30] Strengthening Forensic Science in the United States: A Path Forward, Committee on Identifying the Needs of the Forensic Sciences Community, National Research Council, 2009.

Update

Forensic Science International
Volume 287, Issue , June 2018, Page 217

DOI: https://doi.org/10.1016/j.forsciint.2018.04.001

Forensic Science International 287 (2018) 217

Contents lists available at ScienceDirect

Forensic Science International

journal homepage: www.elsevier.com/locate/forsciint

Corrigendum

Corrigendum to "How important is it to consider target properties and hematocrit in bloodstain pattern analysis?" [FSI 266C (2016) 178–184]

Sungu Kim, Yuan Ma, Prashant Agrawal, Daniel Attinger*

Department of Mechanical Engineering, Iowa State University, Ames, IA 50011, USA

The authors regret that on Table 3, the reporting values of roughness for a range of substrates, has a typo for the roughness unit, mentioning [mm] instead of the correct magnitude in [μm].

The authors would like to apologise for any inconvenience caused.

DOI of original article: http://dx.doi.org/10.1016/j.forsciint.2016.05.015
* Corresponding author.
E-mail address: attinger@iastate.edu (D. Attinger).

http://dx.doi.org/10.1016/j.forsciint.2018.04.001